AN APPROACH TO STIMULATION OF OCEAN MULTIPATH PHENOMENA FOR SONAR TRAINING DEVICES

MICHAEL F. STURM and IRWIN S. FROST
Honeywell
Marine Systems Division

To meet the increasing threat imposed by well-equipped, modern submarines, active and passive sonar systems with highly sophisticated signal processing and display subsystems must be developed. Training of sonar operators to use these systems effectively requires simulation of actual operations whenever possible. This can be achieved by providing a training system that: (1) simulates operational equipment, or (2) stimulates the actual tactical hardware. The trainer must present the trainee with the same operating situation that he will encounter in real-world combat conditions, including the ocean acoustic model.

Training system models of the ocean acoustic environment must be adequate to represent the new sonar systems, with their increased sophistication and improved signal processing capabilities. Consequently, new and more complete acoustic environmental models, which can run in real-time, must be developed for both active and passive mode sonar systems trainers. To stay within Navy budgets, however, innovative, cost-effective concepts and designs are required for the models, as well as the stimulation hardware.

The amount of nontactical hardware required for the development of sonar training devices using stimulation techniques is roughly proportional to the number of acoustic paths that must be simulated. The sounds of all acoustic paths between a source and a receiver must be generated, frequency-shaped, attenuated, and inverse-beamformed. A reduction in the total number of acoustic paths to a subset sufficient for stimulation, while retaining the inherent attributes of the ocean multipath phenomenon and sonar capabilities, permits effective training with a minimum amount of nontactical hardware.

The objective of this paper is to discuss a concept and associated analytic processes developed for use in sonar training devices to provide high-fidelity simulation of ocean multipaths. It is shown that this technique can be used to represent the total acoustic field, using two equivalent multipath subsets.

OCEAN ACOUSTICS

Accurate representation of the acoustic field between any two points in the ocean environment requires the consideration and accurate representation of all major contributing acoustic paths between these points. As the whole is the sum of all its individual parts, the total acoustic field is the sum of the individual multipath contributions. It is well-known that, between any two spatial locations, acoustic energy can propagate along many individual paths, the nature of which is solely dependent upon the sound velocity structure of the medium itself. Typical examples of this phenomenon are illustrated in the acoustic ray diagrams and associated sound velocity profile structures shown in Figures 1 and 2. The individual ray paths joining any two points in the medium are referred to as eigenrays. It is the summation of the acoustic characteristics of each of the individual eigenray intensities that determines the field intensity at a given location in the ocean.

The summation of these eigenrays produces such well-known ocean characteristics as multipath interference regions and convergence zones. Figure 3 illustrates the acoustic field enhancement, a decrease in propagation loss, due to the convergence of the individual eigenrays.

Since it is not within the scope of this paper to delineate acoustic ray theory, a less rigorous, yet illustrative, example will be used to introduce the subject simulation problem and solution.

Consider the simplified two-boundary image model geometry shown in Figure 4. For illustrative purposes, multipaths between the source and receiver are assumed to be straight lines; six individual paths are shown. The total acoustic field (assuming unity surface reflection and constant sound speed) at any spatial coordinate is represented by the coherent sum of each individual multipath and is analytically given by,

$$\psi = \frac{e^{ik^*R_1}}{R_1} - \frac{e^{-ik^*R_2}}{R_2}; \quad R < 1000 \text{ yd}$$

$$\psi = \frac{V_3^*(\theta_3)e^{-ik^*R_3}}{R_3} - \frac{V_4^*(\theta_4)e^{-ik^*R_4}}{R_4} - \frac{V_5^*(\theta_5)e^{-ik^*R_5}}{R_5} + \frac{V_6^*(\theta_6)e^{-ik^*R_6}}{R_6};$$

$$R > 1000 \text{ yd}$$

$$N_W = 20 \log |\psi|$$

where

k^* = propagation constant

$R_1 \ldots R_6$ = length of each path

$V_3^* \ldots V_6^*$ = bottom reflection coefficient corresponding to bottom grazing angles $\theta_3 \ldots \theta_6$

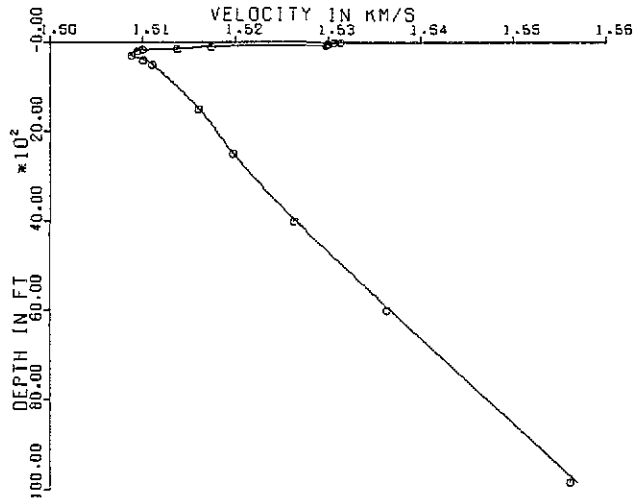

Figure 1a. Typical Sound Velocity Profile

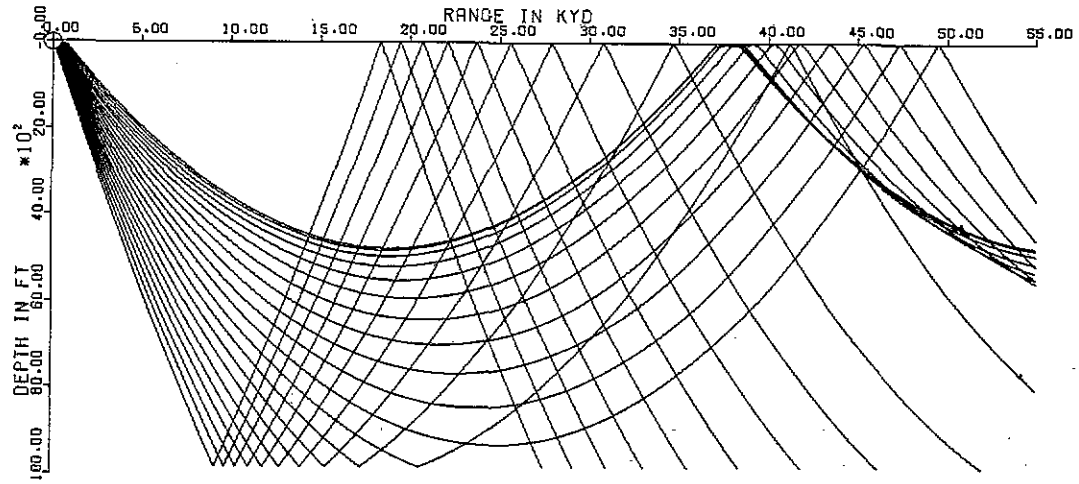

Figure 1b. Typical Acoustic Ray Plot

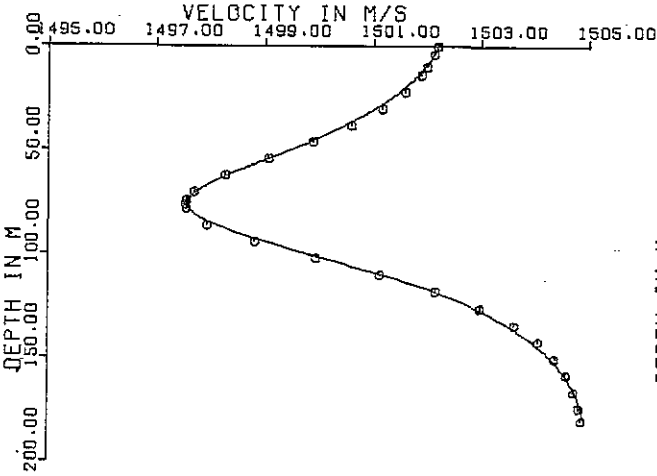

Figure 2a. Typical Sound Velocity Profile

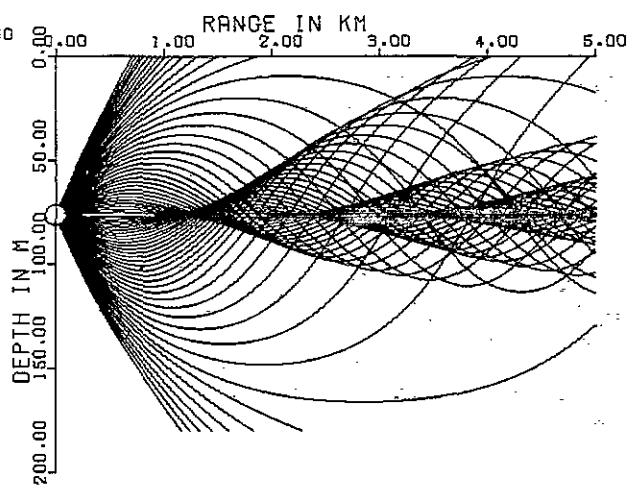

Figure 2b. Typical Acoustic Ray Plot

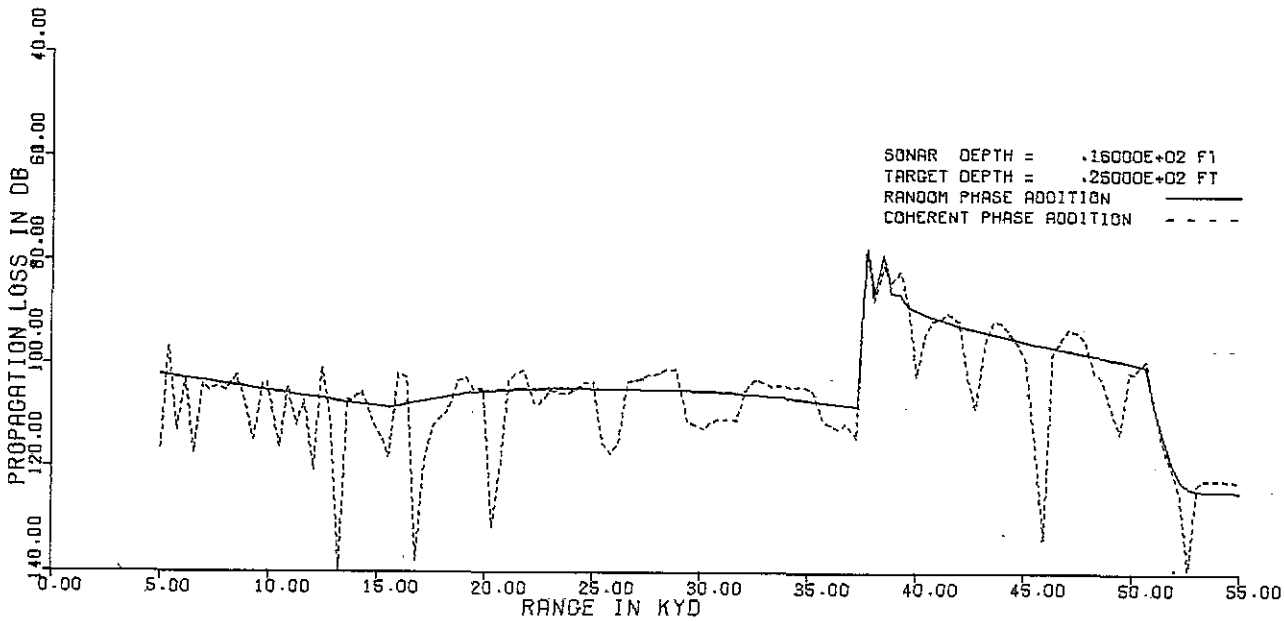

Figure 3. Typical Propagation Loss Plot Illustrating Convergence Zone

Information associated with each of these multipaths includes intensity (spreading and absorption loss, bottom and surface loss), phase, arrival angle, and travel time or differential travel time. In this example, path length and time are functionally equivalent, since a constant speed of sound is assumed. In the more rigorous sense, this is not true, since the actual acoustic energy travels along ray paths in a medium at a continuously varying sound speed.

Figure 5 illustrates a typical propagation loss output from the aforementioned image model. To provide high-fidelity simulation of ocean phenomena commensurate with the operational capabilities of the tactical hardware, the various attributes of multipath propagation, as summarized above, must be considered for effective sonar training. If the tactical hardware is sensitive to the effects of multipath phenomena, these effects must be simulated to a fidelity equivalent to the hardware capabilities.

APPLICATION

Generically speaking, sonar or nonsonar training devices can be divided into two basic categories: (1) full simulators, not employing tactical hardware; in these devices, visual and aural trainee presentations are almost completely under the control of mathematical processes; and (2) stimulators, in which synthetic signals are

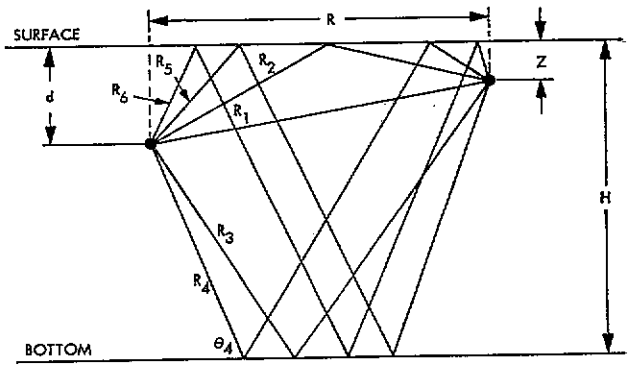

Figure 4. Two-Boundary Image Model Geometry

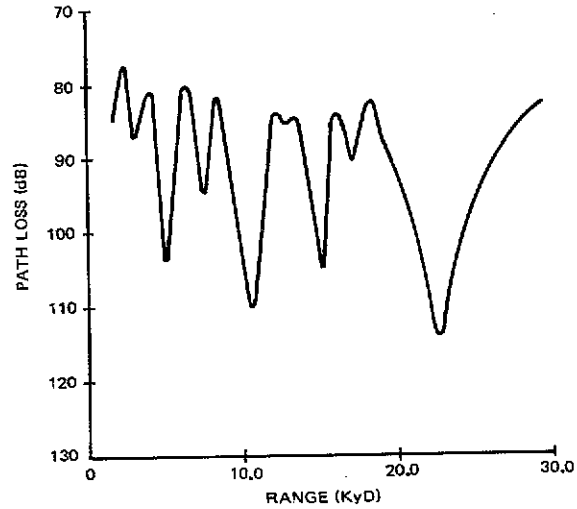

Figure 5. Typical Two-Boundary Image Model Propagation Loss Output

injected at some point into the tactical hardware under the control of mathematical processes.

The process of achieving a cost-effective trainer design often includes development of synthetic signals that do not completely map real-world phenomena but are "acceptable for training." For a sonar training system using stimulation techniques, the synthetic signals must be more nearly representative of the real-world acoustic signals if the tactical equipment is to be "fooled." The further the point of injection is moved to the front end of the system, the greater the fidelity required of these synthetic acoustic signals.

In a sonar trainer employing full simulation or stimulation with injection after the beamformer, effects of multipath phenomena can be functionally simulated and represented in a purely analytic manner, irrespective of the complexity of the mathematical processes required, as shown in Figure 6.

A sonar trainer that uses synthetic signal injection points at either the input or output of the array sensor pre-amps and depends on the sensitivity of the system to multipath signals requires the use of an inverse beamformer and associated signal generator for each target multipath combination, as illustrated in Figure 7. The inverse beamformers are required to time-orient the synthetic signals in both the vertical and azimuthal planes so that the spatial geometry of the array sensors is accounted for prior to signal injection into the tactical hardware beamformers.

ALGORITHM OVERVIEW

The primary computer program used to develop the concepts presented in this paper is the Navy Interim Surface Ship Model (NISSM) II (Ref. 1). NISSM was developed by Dr. Henry Weinberg of the Naval Underwater Systems Center at New London, Connecticut, to predict the performance of sonar systems. The program provides, as a function of ocean and system parameters, acoustic ray paths, propagation loss predictions, boundary and volume reverberation, signal-to-noise ratios, and probability of detection outputs, using continuous-gradient ray-tracing techniques. Model assumptions include horizontal ocean boundaries and a non-range-dependent sound velocity profile.

The algorithm developed for selecting "bundled" multipaths is currently automated on a CDC 6600 as part of an in-house NISSM II system. All figures presented in this paper were created from this system.

As mentioned earlier, many eigenrays exist between the source and receiver. Selection of the ray path and associated acoustic information for simulation or stimulation is, therefore, of prime importance. If selected incorrectly, many of the acoustic phenomena required for training could be inadvertently omitted. A typical selection criterion that is sometimes considered is to provide the acoustic information associated with the two strongest eigenrays. This is a good approximation if the selected eigenrays are sufficiently stronger than the remaining ones; however, it is not necessarily a typical situation. Since this type of selection process can produce significant errors in certain instances, it should not be considered the optimal approach. For example, consider the typical plot of propagation loss versus range presented in Figure 8. The solid line represents the coherent summation of path loss along all ray paths. The line broken by circles represents the coherent summation of the path loss using the two strongest rays. More significant than the errors between the two curves is the fact that they do not have the same general shape. Therefore, to provide effective training (again dependent upon the tactical hardware capabilities)

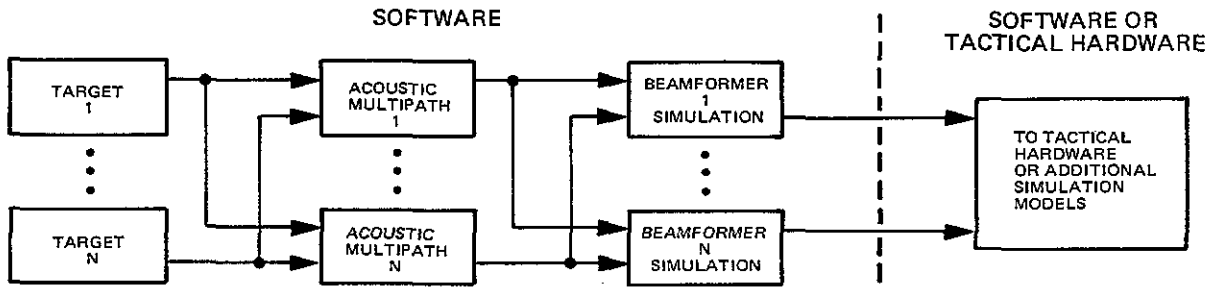

Figure 6. Target/Acoustic Path Function Block Diagram for Simulation or Post-Beamformer Stimulation Implementation

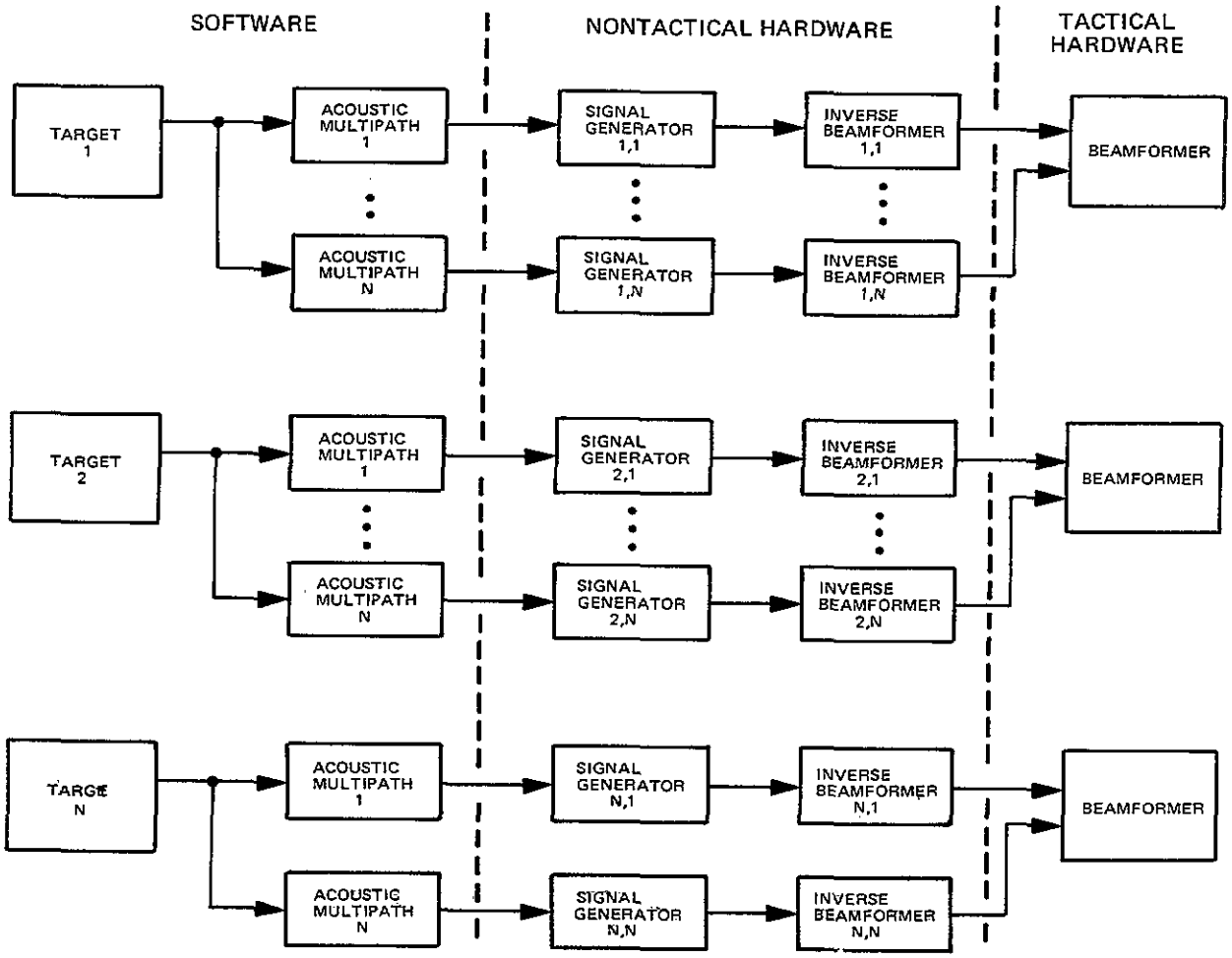

Figure 7. Target/Acoustic Path Function Block Diagram for Pre-Beamformer Stimulation Implementation

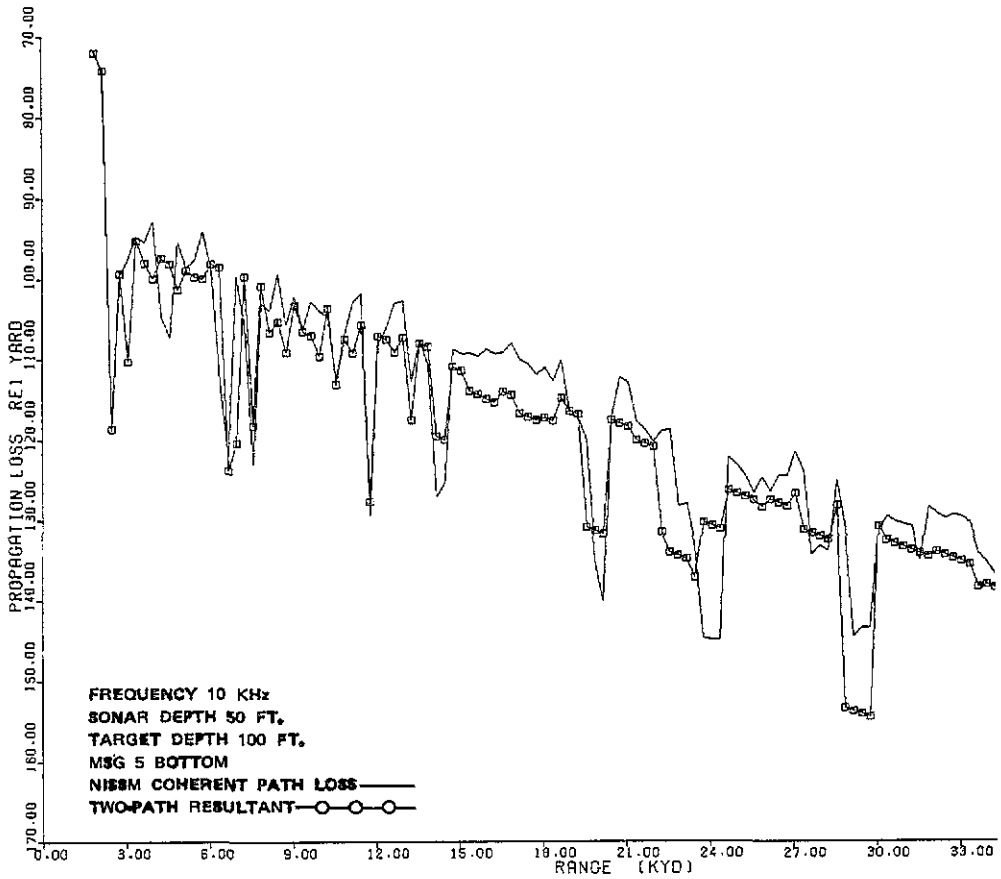

Figure 8. Comparison of NISSM vs Two Strongest Rays for Mediterranean Profile - Summer

a more accurate, cost-effective representation of the acoustic field for training systems must be provided. The technique provided in this paper provides the required cost-effective fidelity, using a process that permits representation of the total acoustic field by two equivalent multipath "bundles." This process is described in the remainder of the paper.

BUNDLING ALGORITHM

The subject bundling algorithm uses the effective coherent propagation loss, which is calculated from:

$$N_{eff} = -20.0 \log_{10} \left| \sum_j 10^{-0.05 N_j} e^{i(2\pi f t_j + \zeta_j)} \right|$$

where

N_j = propagation loss for the j^{th} eigenray (dB)

f = frequency (Hz)

t_j = travel time for the j^{th} eigenray (seconds)

ζ_j = discrete phase angle change of the j^{th} eigenray due to boundary interactions (radians).

Figure 9 illustrates the bundling algorithm in flowchart form. The algorithm to be used (except in a caustic region) is computed as follows:

a. *Calculate the coherent propagation loss* of all upward-going eigenrays, N_u.

b. Calculate the coherent propagation loss of all downward-going eigenrays, N_d.

c. Select the strongest upward eigenray ($j = j_u$) and the strongest downward eigenray ($j = j_d$), combine these coherently, and obtain N_1, using Equation 1.

d. Select the strongest upward eigenray ($j = \hat{j}$) such that $\zeta_{\hat{j}} \neq \zeta_{j_u}$

e. Coherently combine the $\hat{j}$ eigenray path with the j_d eigenray path, N_2, in accordance with Equation 2.

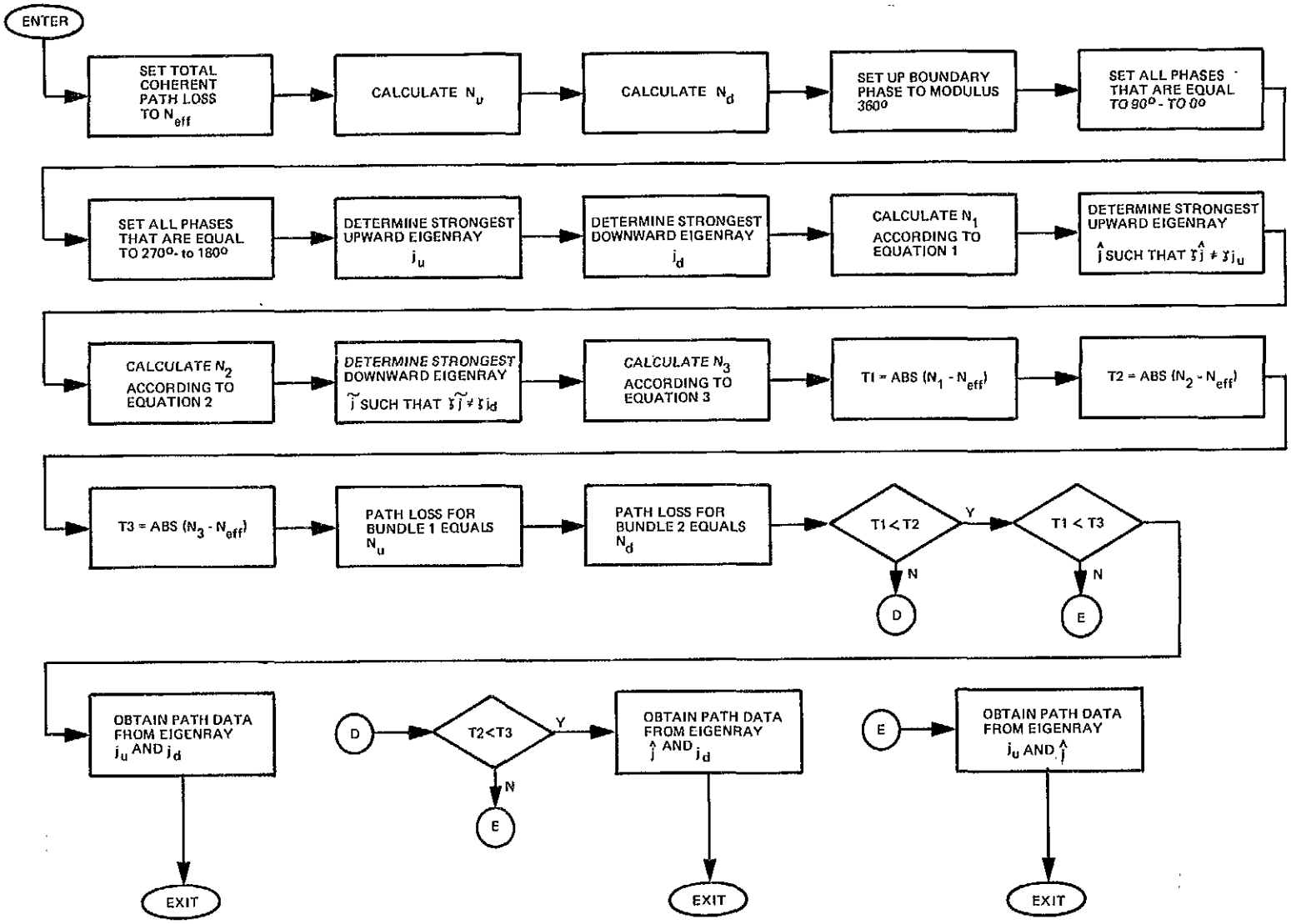

Figure 9. Bundling Algorithm Flow Chart

f. Select the strongest downward eigenray ($j = \tilde{j}$) such that $\zeta_{\tilde{j}} \neq \zeta_{j_d}$

g. Coherently combine the $\tilde{j}$ eigenray path with the j_u eigenray path, N_3, in accordance with Equation 3.

h. Values of N_u and N_d provide the propagation loss values for the two bundled paths.

Associated acoustic information required for simulation/stimulation includes angles and time of arrival and discrete phase information, which are obtained from the eigenray paths by using the following criteria:

(1) If N_1 is closest to N_{eff}: Paths j_u and j_d

(2) If N_2 is closest to N_{eff}: Paths $\hat{j}$ and j_d

(3) If N_3 is closest to N_{eff}: Paths $\tilde{j}$ and j_u.

Figures 10 through 12 illustrate the outputs obtained by using the aforementioned algorithms. The parameters for Figure 8 and 10 are identical, serving to illustrate the higher fidelity obtained by using the bundling algorithms, as opposed to selecting the strongest eigenrays.

Figure 11 illustrates typical results obtained in well-defined interference regions. Once again, use of the bundling algorithms provides excellent correlation with the primary NISSM II output.

For a caustic region typically associated with convergence zones, NISSM II uses a -90 degree phase shift. For the bundling algorithm, once N_u and N_d are calculated, it has been shown that the caustic phase shift is no longer required. Hence, phase information provided for each bundled path is represented by either 0 or 180 degrees to account for the surface boundary phase shifts. To use the aforementioned algorithms within a caustic region, the following step should be included after Step b:

b1. Modify all phase shifts to account for surface boundaries only; delete the caustic phase shift of -90 degrees.

Figure 13 illustrates the application of the caustic correction. Once again, the output of the NISSM II model and that provided by the bundling algorithm are well correlated.

EQUATIONS

$$N_1 = -20.0 \log_{10} \left| \text{of} \; 10^{-0.05N_u} \cdot e^{i(2\pi f t_{j_u} + \zeta_{j_u})} + 10^{-0.05N_d} \cdot e^{i(2\pi f t_{j_d} + \zeta_{j_d})} \right| \quad (1)$$

$$N_2 = -20.0 \log_{10} \left| \text{of} \; 10^{-0.05N_u} \cdot e^{i(2\pi f t_{\hat{j}} + \zeta_{\hat{j}})} + 10^{-0.05N_d} \cdot e^{i(2\pi f t_{j_d} + \zeta_{j_d})} \right| \quad (2)$$

$$N_3 = -20.0 \log_{10} \left| \text{of} \; 10^{-0.05N_u} \cdot e^{i(2\pi f t_{j_u} + \zeta_{j_u})} + 10^{-0.05N_d} \cdot e^{i(2\pi f t_{\tilde{j}} + \zeta_{\tilde{j}})} \right|. \quad (3)$$

REFERENCE

1. Weinberg, H., Navy Interim Surface Ship Model (NISSM) II, NUSC Technical Report No. 4527, October 1973.

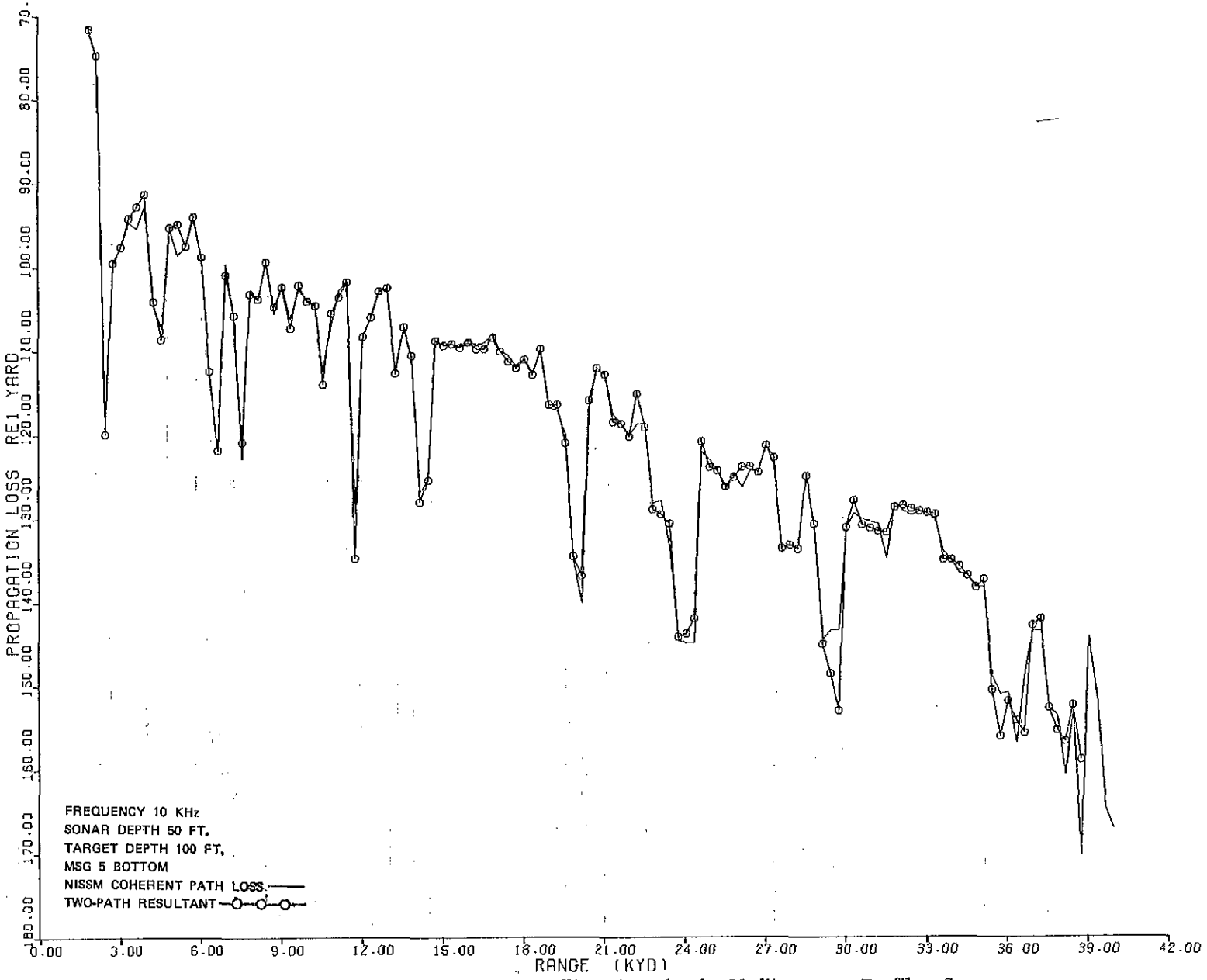

Figure 10. Comparison of NISSM vs Bundling Algorithm for Mediterranean Profile - Summer

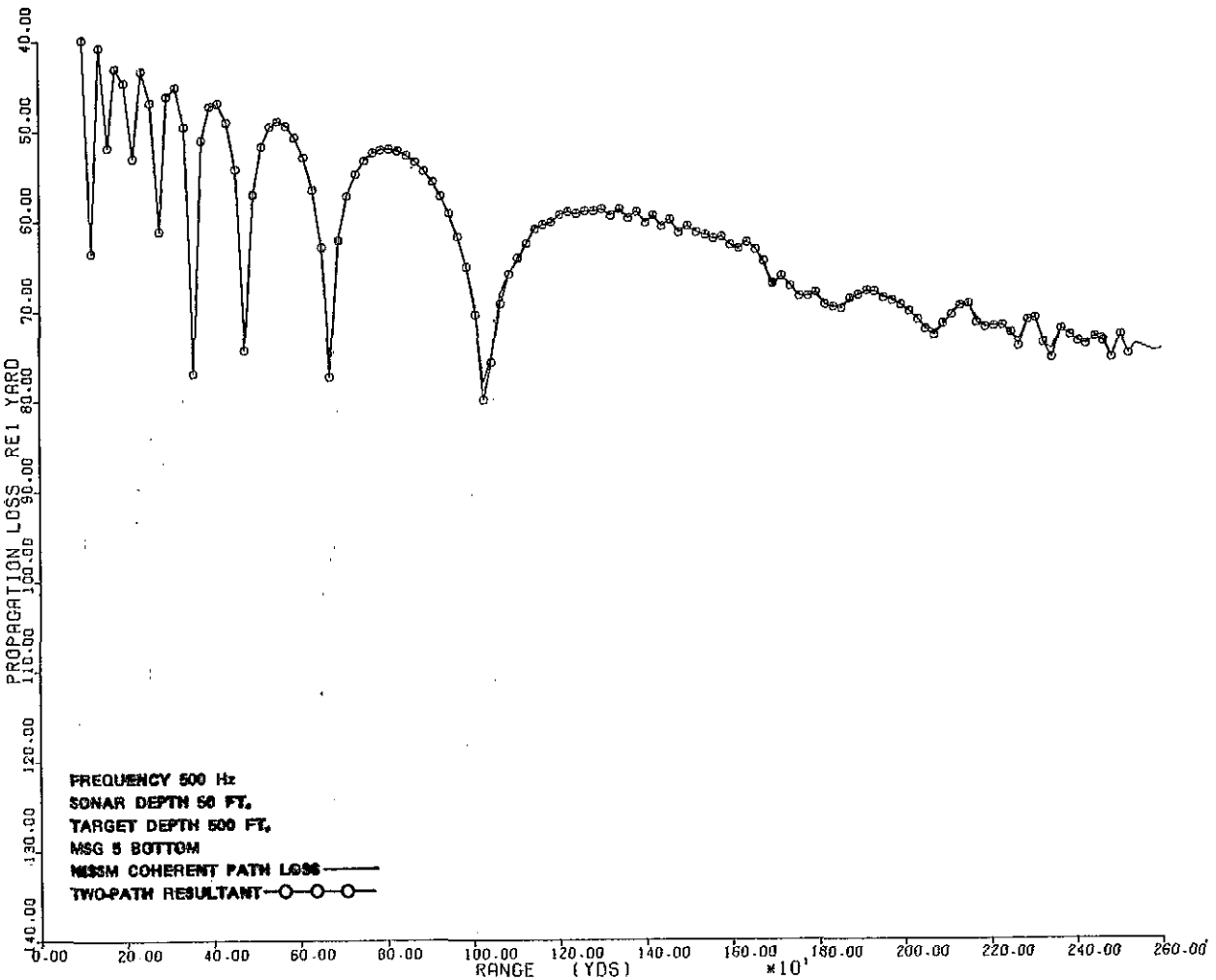

Figure 11. Comparison of NISSM vs Bundling Algorithm for Mediterranean Profile – Summer – Multipath Interference Region

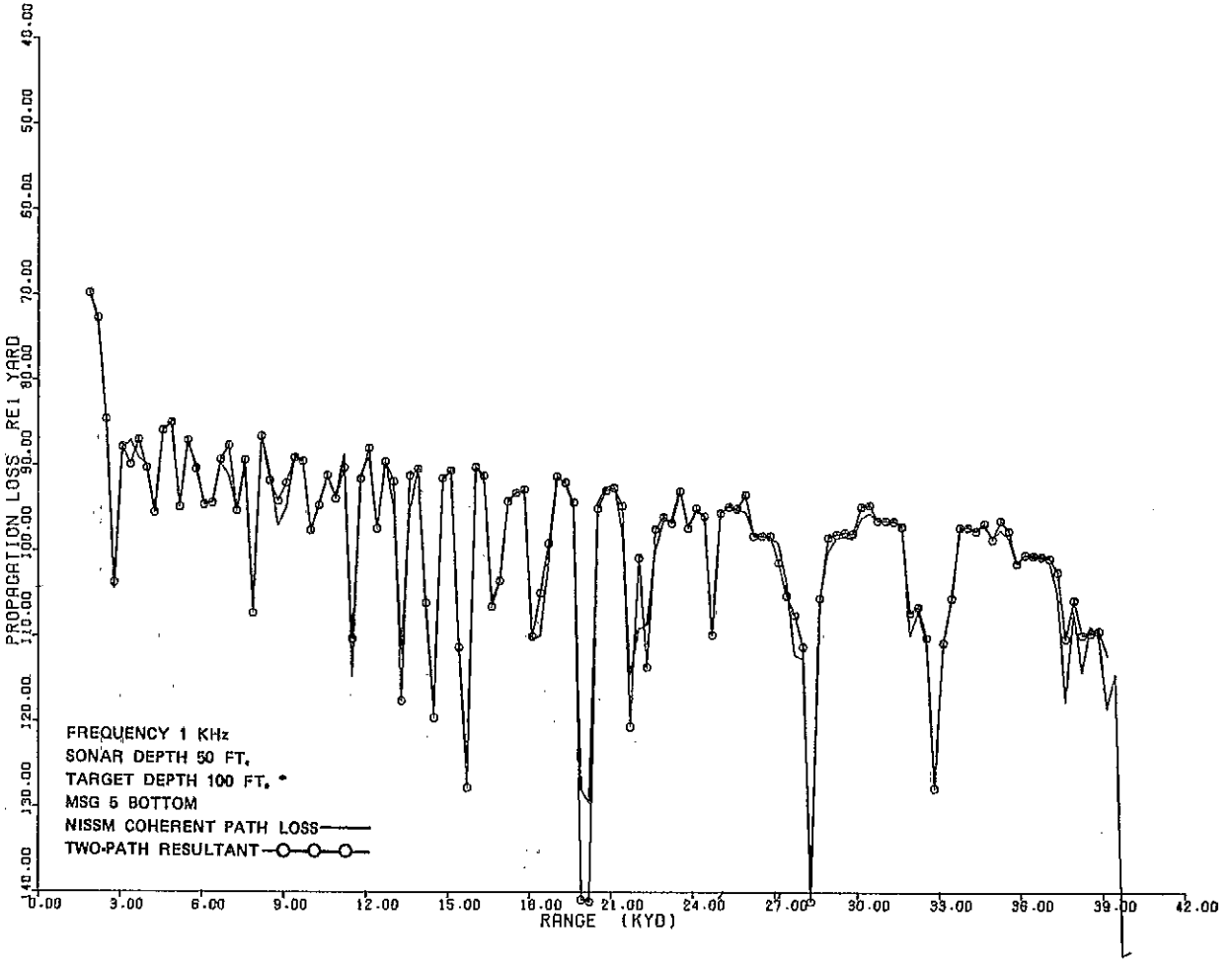

Figure 12. Comparison of NISSM vs Bundling Algorithm for Mediterranean Profile - Summer

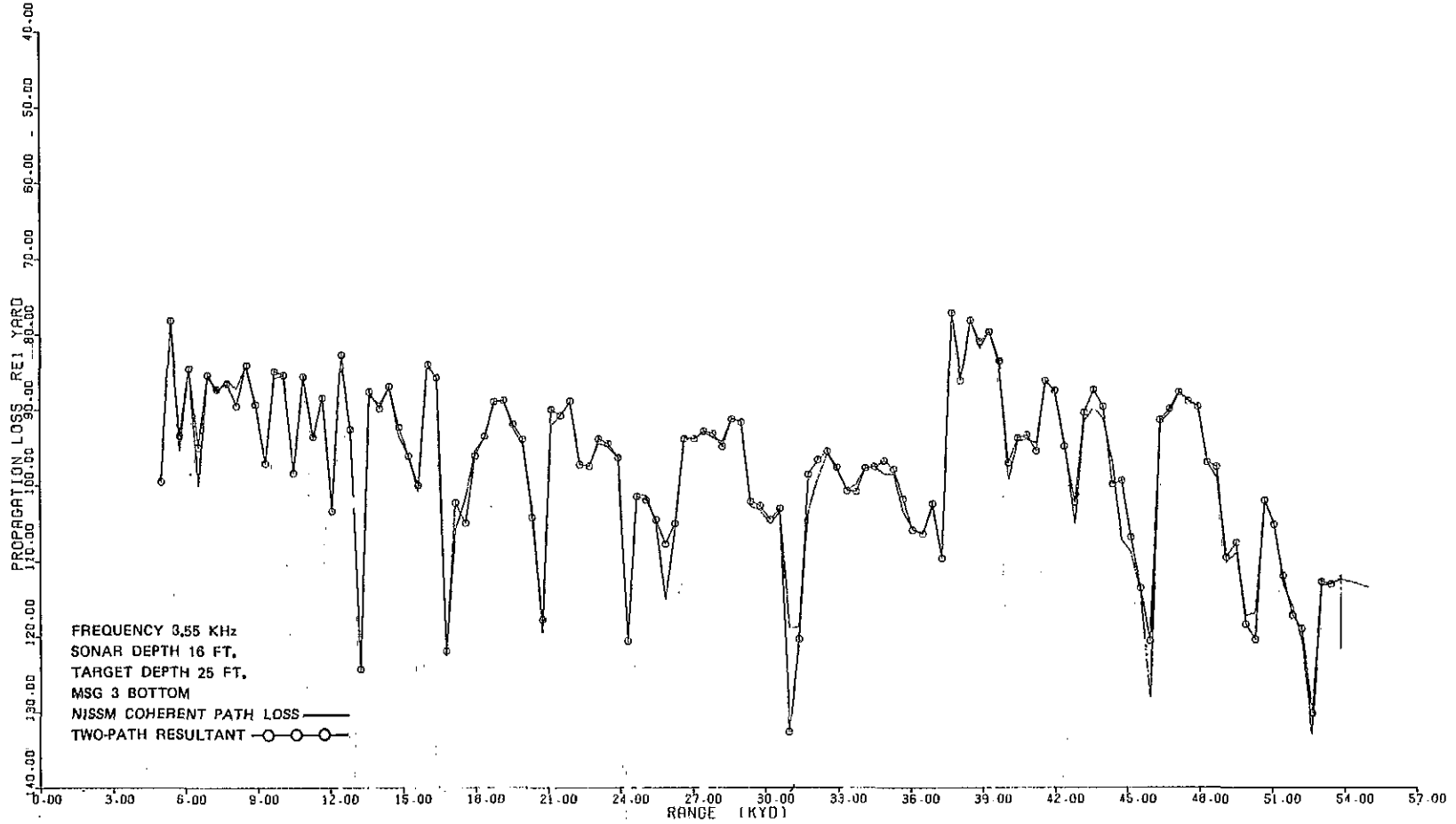

Figure 13. Comparison of NISSM vs Bundling Algorithm for Tyrrhenean Sea - Convergence Zone

ABOUT THE AUTHORS

MR. MICHAEL F. STURM is a Principal Development Engineer in the trainer modeling group at Honeywell, Marine Systems Division California Center. He is Lead Analyst, responsible for design and development of the real-time simulation models for the FBM SOT trainer. Since joining Honeywell in 1971, he has had various responsibilities in the design and development of real-time simulation models for sonar training devices, including Devices 14E23, 14E24, 21B64, and BQR-21 ULT. He has also been responsible for conducting advanced real-time sonar simulation analysis on a variety of Honeywell-sponsored IR&D programs. Prior to joining Honeywell, Mr. Sturm was at Motorola, Microdesign, and J.D. Katelle. He received the B.S. degree in mathematics from Polytechnic Institute of Brooklyn, and the M.S. degree in applied mathematics from California State University, Los Angeles.

MR. IRWIN S. FROST supervises the simulation modeling group at Honeywell Marine Systems Division California Center. He has been involved in a wide spectrum of underwater acoustic research and development, including the design and development of operational sonar systems. Since joining Honeywell in 1967, Mr. Frost has been responsible for the design and development of real-time simulation models for sonar training devices, including Devices 14E19, 14E23, 14E24, 14E25, 14E25A, 14E27, 21B64, AN/BQR-21 ULT, and FBM SOT. He has also been responsible for numerous Honeywell IR&D programs associated with simulation and stimulation of underwater acoustic phenomena as applied to sonar training devices. He was a teaching and research assistant in the Physics Department at University of Massachusetts, and conducted research in the area of low-energy ion-atom collisions. Prior to joining Honeywell, he was with Sperry Gyroscope for six years. He has published two papers, holds one copyright, and has taught underwater acoustics courses at Honeywell. He received the B.A. degree in physics from Hunter College in New York City and the M.S. degree in physics from the University of Massachusetts.